



# Experimental investigation on the springback of AZ31B Mg alloys in warm incremental sheet forming assisted with oil bath heating

San Zhang<sup>1,2</sup> · G. H. Tang<sup>3</sup> · Zhen Li<sup>1</sup> · Xiangkui Jiang<sup>1</sup> · KeJie Li<sup>4</sup>

Received: 12 November 2019 / Accepted: 22 June 2020 / Published online: 5 July 2020  
© Springer-Verlag London Ltd., part of Springer Nature 2020

## Abstract

Magnesium (Mg) alloy sheets have attracted considerable attention as one of the most promising lightweight structural materials for weight reduction-oriented industries owing to their excellent properties compared with conventional materials. However, basal-textured Mg alloy sheets exhibit extremely inferior formability at room temperature due to their hexagonal close-packed structure and the limited number of active slip systems. Herein, an innovative warm incremental sheet forming assisted with oil bath heating approach to form difficult-to-form metal materials is proposed. To examine the forming quality of the approach, using springback as an evaluation index, a sequence of tests was conducted while forming AZ31B Mg alloy sheets according to a central composite design including response surface methodology and analysis of variance. The results indicated the approach was able to form Mg alloy sheets with great feasibility. The forming temperature (A), forming angle (B), step depth (C), and sheet thickness (D) are substantial factors that affect the springback, whereas the tool diameter (E) has a much less influential role compared with the individual effects of the other parameters, and the reasons for these results are explained. All the remaining interactive terms are substantial interactive factors except the AB, AE, BE, and CD terms, and a quadratic regression model gives the best fit with a 95% confidence level for springback. It was also indicated from the optimization results that to achieve a minimum springback value, the 166.3 °C forming temperature, 50.4° forming angle, 0.22-mm step depth, 1.18-mm sheet thickness, and 11.5-mm tool diameter should be selected.

**Keywords** Warm incremental sheet forming · Springback · Oil bath heating · AZ31B Mg alloys · Response surface methodology

## 1 Introduction

Magnesium (Mg) alloy sheets, such as AZ31B, have attracted considerable attention as one of the most promising lightweight structural materials for weight reduction-oriented industries, e.g., automotive and aerospace industries, owing to their excellent properties compared with conventional materials, such as a low density, a high specific strength, a high specific stiffness, and abundant resources [1–3]. Mg alloys have also been applied for a large variety of innovative consumer electronic products due to their excellent mechanical properties, resistance to aging and corrosion, good vibration-damping, and electromagnetic shielding performance [4]. Therefore, utilizing them in innovative forming technologies provides the chance for numerous new products. Flexible forming technologies, particularly incremental sheet forming (ISF), have been newly proposed to meet the requirements for manufacturing small series of parts and multi-variety products with complex structures [5–7]. The application

✉ San Zhang  
ucaszhangsan@163.com

<sup>1</sup> School of Automation, Xi'an University of Posts & Telecommunications, No. 618, West Chang'an Avenue, Chang'an District, Xi'an 710121, People's Republic of China

<sup>2</sup> National Demonstration Center for Experimental Information & Control Engineering Education, Xi'an University of Technology, No. 5, South Jinhua Road, Beilin District, Xi'an 710048, People's Republic of China

<sup>3</sup> MOE Key Laboratory of the Thermo-Fluid Science & Engineering, Xi'an Jiaotong University, No. 28, Xianning West Road, Beilin District, Xi'an 710049, People's Republic of China

<sup>4</sup> College of Mechanical & Electrical Engineering, Taizhou Vocational & Technical College, No. 788, Xueyuan Road, Jiaojiang District, Taizhou 318000, People's Republic of China

of ISF on Mg alloy sheets is considered to be an excellent solution for obtaining innovative sheet metal products. The ISF is completely different from conventional methods: it uses a series of small localized deformations and changes the shape of the parent metal sheet without expensive and dedicated dies compared with other forming processes, and it also belongs to the category of advanced manufacturing technology [8–13].

At present, increasing attention has focused on the application of the ISF technology for Mg alloy sheets. However, the forming ability of those materials is extremely poor at ambient temperature due to the hexagonal close-packed (HCP) crystal structure, strong basal crystallographic texture, and strong texture evolution during the plastic deformation process [4, 8, 14, 15]. These main problems contribute to higher springback values and lower dimensional precision [16]. In particular, a great deal of Mg alloy materials cannot be formed to produce quality final products.

Over the past few decades, to overcome these challenges, a large number of scholars and engineers have performed a substantial research and have tried to improve the forming ability and forming quality of Mg alloys. Several studies have indicated that the room temperature formability of Mg alloys strongly depends on texture and deformation twinning, and nonbasal slip systems such as prismatic and pyramidal slip systems can be activated through temperature increases [16–18]. Therefore, a promising solution is to increase the material formability and geometrical accuracy of the AZ31B Mg alloy sheet by elevating the forming temperature. Warm incremental sheet forming (WISF) technologies for elevating the forming temperature have been applied to improve the forming ability and geometrical accuracy of Mg alloy sheets, and they are quite useful for forming materials that exhibit poor overall ductility at room temperature. To date, a large quantity of heating approaches for WISF has been proposed based on the ISF methods in previously published works. It is not possible to conduct an extensive review of the literature on the topic in this short introduction. A detailed review of the experiments and theoretical studies conducted on heating strategies for warm incremental sheet forming is presented in [10, 19–21]. However, heating strategies in the aforementioned literature either have too complex of an equipment structure or too high of a maintenance cost. To the best of our knowledge, WISF assisted by the oil bath heating approach involves a fairly simple structure and very low cost, yet few experimental investigations on this approach have been conducted worldwide. In addition, ISF is not extensively used in the industrial field because of its poor forming precision. One of the important reasons for the lack of implementation is that springback is one of the inherent shortcomings of all ISFs and one of the main factors that influence the forming precision during the incremental forming process [22]. As with numerous factors, decreasing the springback deviation is also one of the most important methods to improve the forming precision, and studies on springback behavior are not yet sufficient and adequate.

Therefore, one of the main objectives of the current work is to explore an innovative WISF approach with global heating by using an oil bath device as a heat source to form Mg alloy sheets or other hard-to-form metallic materials. Then, an experimental investigation on oil bath heating-assisted WISF while forming the AZ31B Mg alloy sheet is carried out based on the design of experiments (DOE). In particular, another important topic is that springback is the most significant source of geometric deviation, and the effects of processing parameters, i.e., the step depth, forming angle, forming temperature, tool diameter, and sheet thickness, on springback are estimated and optimized according to the response surface methodology (RSM) and analysis of variance (ANOVA). The empirical correlation is well defined through a quadratic model, as it includes all the significant terms that affect springback.

## 2 Theoretical background

### 2.1 Springback analyses in the ISF process

Springback in the ISF process is an undesirable phenomenon in which the final contour of the metal sheet deviates from its desired contour when the forming loads are removed from the contact zone after the forming operation is performed. In traditional sheet forming presses, e.g., stamping and forging, the contact area between the sheet and the forming tool throughout the forming processes is quite large, and springback is developed after the forming tool is removed [23–25]. However, the contact area between the sheet and the forming tool is small in the flexible ISF process, and the deformed contour generally needs to be trimmed in order to produce the final contour [10]. Therefore, springback in the ISF process can be divided into three main categories: type I, continuous local springback, which occurs simultaneously with the displacement of the tool; type II, global springback, which occurs after the loads are removed and released from the forming fixture; and type III, global springback, which arises after trimming (if done) [10]. In the present work, type II is investigated because this form of springback is more pronounced in the ISF process than the other two types.

According to the different locations where springback occurs, type II springback is further divided into two groups: sidewall springback and bottom wall springback, as illustrated in Fig. 1a, b. There are five sections in the sidewall springback: in the AB section, the nonprocessing transition section, known as the bending effect, has a negative value of springback; it decreases with increasing forming depth and then reaches a maximum value at point B in the section; in the BC section, the springback is also a negative value and reduces from a maximum value to zero corresponding to point B to point C; in the CD section, the positive springback value occurs at point C and increases with increasing forming depth, then reaches a maximum value at point D; in the DE section,

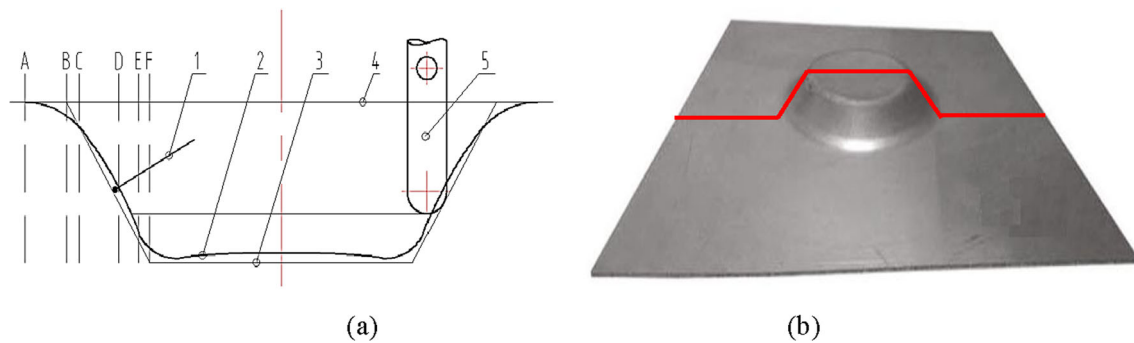


**Fig. 1** Schematic diagram (a) and photograph (b) of the sidewall springback and bottom wall springback (1, dial gauge; 2, actual contour; 3, ideal contour; 4, initial sheet; and 5, forming tool)

positive springback reaches a maximum value, then tends to stabilize and hold constant; and in the EF section, the positive springback decreases with increasing forming depth. The springback behavior is simple in the bottom wall and is known as the pillow effect, and the positive springback increases gradually with increasing forming depth.

## 2.2 Methodology of the springback measurement

As mentioned before, different section locations in the actual contours, i.e., the sidewall and bottom wall section, have different springback values. The same processing parameters also have different effects on the springback. However, compared with the bottom wall springback, the sidewall springback has a much greater effect on the final product quality. Therefore, the experimental investigation on the sidewall springback is presented in the current work. A simple method for establishing the degree of springback at a particular predefined point is simply to measure the difference between the  $z$  values along the vertical direction in the desired and actual contours. However, a more accurate and simple method is to determine the distance of the surface normal to each predefined point in the desired contours to the point where it intersects with the actual contours. The distance between the two contours is considered to be the springback. In the current work, to measure the magnitude of the springback produced by the new WISF process after finishing the entire process and unloading the final forming part, a dial gauge is used to determine the springback of the horizontal cross-sectional contours on the sidewall. It is worth noting that the probe of the dial gauge remains perpendicular to the surface of the desired contours by adjusting the direction of the dial gauge. Then, the maximum value of the springback is recorded at the half-height of the sidewall, as illustrated in Fig. 1a. For repeatability, each measuring value was determined three times to obtain an average value at the fixed location in the measuring process. The average value of the springback is calculated using the following formula:

$$S_s = \sum S_i / n \quad (1)$$

where  $S_s$  is the average springback of the sidewall,  $S_i$  is the maximum springback,  $i = 1, 2, 3$  is the  $i$ th measurement, and  $n$  is the total number of measurements.

## 3 Experimental setup and details

In this section, the machine tool used along with the clamp system, the sheet metal material, and its main chemical compositions are described. Moreover, the adopted statistical analysis and tool path are presented in detail.

### 3.1 Experimental materials

The adopted material in the present work is AZ31B Mg alloy due to its frequent applications in sheet metal forming industrial fields, and blank square sheets with dimensions of 150 mm × 150 mm are prepared with different thicknesses for the WISF experiments, as demonstrated in Fig. 2c. The AZ31B Mg alloy material has a strong basal texture structure, and its chemical composition has also been tested, as listed in Table 1.

### 3.2 Experimental setup and procedure

The WISF experiments are carried out with a traditional 3-axis vertical CNC milling machine tool (model GD650, supplied by Nanjing Gaochuan Sikai Numerical Control Equipment Manufacturing Co., Ltd.), as illustrated in Fig. 2a. A custom-developed, blank-holding setup with an oil bath-assisted apparatus is fabricated to implement global oil bath heating of the AZ31B Mg alloy sheet. It is conducted in a manner similar to a typical oil bath heating method, and the photograph with an essential and brief explanation of the new setup is also presented in this work, as illustrated in Fig. 2b. A detailed and enlarged photograph of the WISF process assisted with the oil bath heating device is illustrated in Fig. 2d.

A schematic diagram of the special fixture with oil bath heating is schematically illustrated in Fig. 3. A square metal

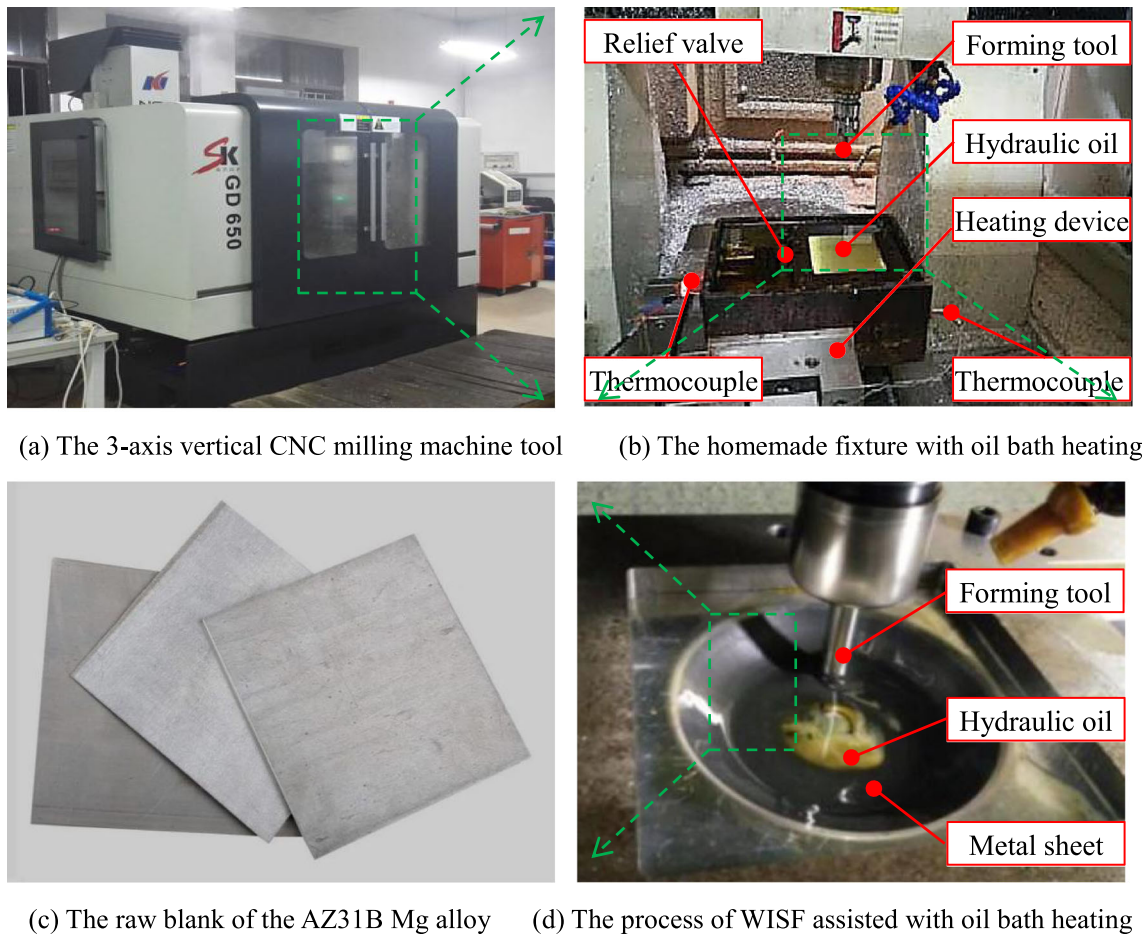


**Fig. 2** a–d The photographs of the related experimental devices and the raw blank materials of the WISF

container was used as the basic framework, and the heating belt and thermal insulating bandage were covered at the interior and exterior walls of the metal container to provide an easy and hard path for heat conduction, respectively. The hydraulic oil stored in the container was heated through an electric heating device (omitted from the figure), and the oil bath temperature could be measured with four thermocouples, which were uniformly installed on the container wall. Then, the electric heating device and four thermocouples were made up of a self-adapted closed-loop temperature control system with a proportion-integration-differentiation controller. Due to spatial reduction during the forming process, to prevent excessive pressure in the metal container, a pressure relief valve (omitted from the figure) was fixed on the container wall through the connection. An initial sheet was installed between the upper clamp and the lower clamp with three screw bolts. To prevent liquid from leaking from the containers, seals were

mounted between the container and the lower clamp. The heat brought forth from the oil bath allowed the sheet temperature to increase in the global forming sheet, thus further increasing the forming ability of the metal blank materials. In particular, to ensure temperature homogenization of the metal sheet, the raw metal blank of each experimental run before starting the forming process was also preheated successively at the nominal temperature for 5 min.

Moreover, the tentative test indicated that the sheet temperature and the oil bath temperature were able to achieve equilibrium in 5 min with a mean error range of  $\pm 2.1$  °C and a maximum relative error of less than 1.5% when an AZ31B Mg alloy blank sheet with a thickness of 12 mm and a forming temperature of 300 °C was heated with the help of the oil bath heating setup. Such an error range was acceptable, especially for this maximum extreme condition. In other words, the initial temperature changes caused by different sheet thicknesses

**Table 1** Chemical compositions of the AZ31B Mg alloy sheet (% weight percent)

Element	Al	Zn	Mn	Si	Fe	Ca	Cu	Bi	Mg
Weight %	2.5–3.5	0.6–1.4	0.2–1.0	< 0.1	< 0.005	< 0.04	< 0.05	< 0.005	Bal.

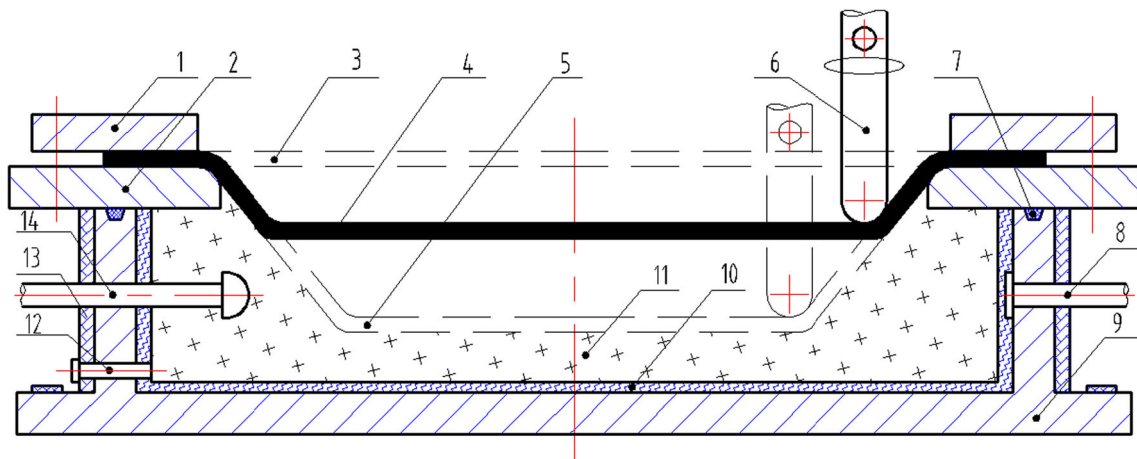


**Fig. 3** A schematic diagram of the experimental setup used for investigation (1, upper clamp; 2, lower clamp; 3, initial sheet; 4, intermediate sheet; 5, final sheet; 6, forming tool; 7, seal; 8, electric heating connection; 9, metal

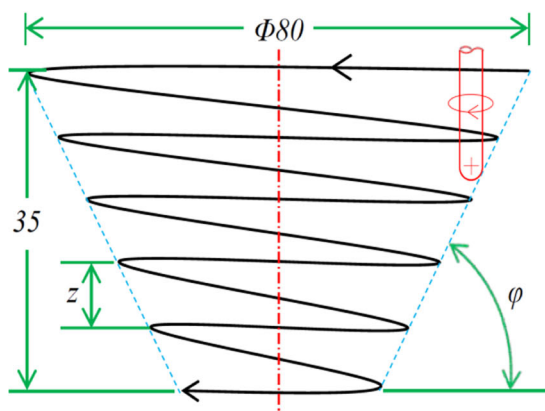
container; 10, heating belt; 11, hydraulic oil; 12, relief valve connect; 13, thermal insulating bandage; and 14, thermocouple)

were negligible. Therefore, it was also sufficient to conduct all the experimental runs because the mean error ranges of the other processing conditions were smaller than the extreme processing condition. It is also worth mentioning that the same idle time between different experimental runs is not a mandatory requirement because the preheating measure is adopted and the preheating time is not less than 5 min before the forming process started.

### 3.3 Tool path description and forming tool

To execute WISF assisted with oil bath heating, the conducted tests were truncated cones with an outer diameter of 80.0 mm, a height of 35 mm in the vertical direction, and an invariable forming angle. The forming strategy adopted was a helical path with a constant step depth per revolution, as illustrated in Fig. 4a. The advantage of this tool path was that no marks were left on the sample. The helical

tool path was continuous with an incremental descent of the tool distributed over the entire surface of a part. The forming processing parameters considered (i.e., the forming temperature, forming angle, step depth, sheet thickness, and tool diameter) in each designated experimental run are listed in Table 3. In addition, other processing parameters, e.g., the feed rate of 100 mm/min and spindle speed of 2000 rpm, were constant in all experimental runs. The tool path data required to form different part geometries were extracted using Unigraphics NX 10.0 software. In the WISF assisted by the oil bath heating process, hemispherical ended and tungsten-cobalt-cemented carbide forming tools with different diameters, as demonstrated in Fig. 4b, were used to form the AZ31B Mg alloy sheets for the tests. To minimize the friction between the tooltip and sheet interface during the forming process, hydraulic oil lubrication was spread before forming to improve the process characteristics. Lubrication also



(a) The spiral tool path of the truncated cone



(b) Photographs of the forming tools

**Fig. 4** a, b A schematic diagram of the spiral tool path and photographs of all the forming tools

enhanced the functionality of the WISF assisted by the oil bath heating process, e.g., the heat dissipation, tool life, and roughness.

### 3.4 Central composite design and statistical analysis

In the current work, to further investigate the effect of the considered parameters on sidewall springback, a design of experiments (DOE) including ANOVA and RSM is applied [26–28]. The RSM was employed to model and optimize springback as the response for the new WISF approach. Because more process parameters are involved in the forming process, a central composite design (CCD) with a single block is chosen to design the experimental matrix in the WISF assisted with oil bath heating. The CCD as a branch of the design type has high reliability for optimization variables and draws mathematical equations that correlate output responses to input variables as single and interaction [28–30]. A five-factor and five-level CCD with a small type is selected to draw a quadratic equation, which indicates the possible achievement of the minimum springback. The quadratic equation represents the correlation among the response to the forming temperature (A), forming angle (B), step depth (C), sheet thickness (D), and tool diameter (E). These independent variables are studied at five different levels coded as  $-\alpha$ ,  $-1$ ,  $0$ ,  $+1$ , and  $+\alpha$ , for which the numerical value of  $\alpha$  is 2.0, and no categorical factor is adopted during the test. The springback of the sidewall is selected as the response of the system and denoted as a forming accuracy index. This design is highly economical when the number of independent factors is more than four. Therefore, it is considered to be an excellent DOE and a total of 26 experimental runs with different combinations of processing parameters are recommended. The test includes 21 noncenter points and an additional 5 center points, which are repeated for 5 runs to assess the reproducibility of the data and experimental error. The processing factors and respective levels in the CCD are summarized in Table 2.

On the existing basis, the functional relation of the response is fitted using the RSM, and the quadratic model is adopted in the present investigation, as demonstrated in Eq. (2).

$$y = \beta_0 + \beta_i \sum x_i + \beta_{ij} \sum x_i x_j + \beta_{ii} \sum x_i^2 + \varepsilon \quad (2)$$

where  $y$  is the response result,  $x_i$  and  $x_j$  are the factor variables that control the independent ISF process parameter,  $\beta_i$  is the coefficient of the linear term,  $\beta_{ij}$  is the coefficient of the quadratic term, and  $\varepsilon$  is the fitting error term.

## 4 Experimental results and discussions

In this section, experimental results and the effects of all the considered parameters on the springback are exhibited and discussed. The regression models for predicting the minimum springback are established, and the optimized experimental parameters for the desired response during the forming processes are obtained through Design Expert 10 trial software.

### 4.1 Experimental results of the CCD sequence

The experiments were carried out according to the run order of the design matrix for WISF assisted with oil bath heating, and some of the final manufactured samples were successfully formed without fracture. In particular, the forming angle was one of the best appearance features of the final manufactured samples. To highlight this feature, five different forming angles were reflected and demonstrated in the selected manufactured samples, as illustrated in Fig. 5. Then, a sequence of test results of different processing variables (i.e., the forming temperature, forming angle, step depth, tool diameter, and sheet thickness) and the corresponding response value (i.e., springback) were recorded, as illustrated in Table 3. In light of the experimental results, statistical analysis was performed to study the effects of each factor on the responses. The response surface regression procedure (Eq. (2)) was applied using the quadratic model to analyze the experimental data obtained.

### 4.2 Development of the regression model

To select the best empirical model to express the correction of the output response and input variables, linear, two-factor interaction, quadratic order, and cubic order regression models were employed to fit the output response of the input factors. In the present work, the quadratic regression model was

**Table 2** Process factors and their respective levels ( $\alpha = 2.0$ )

Levels	Forming temperature ( $t/^\circ\text{C}$ ), A	Forming angle ( $\varphi/^\circ$ ), B	Step depth ( $z/\text{mm}$ ), C	Sheet thickness ( $h/\text{mm}$ ), D	Tool diameter ( $d/\text{mm}$ ), E
$-\alpha$	100	45	0.1	0.6	$\Phi 6$
$-1$	150	50	0.2	0.8	$\Phi 8$
0	200	55	0.3	1.0	$\Phi 10$
$+1$	250	60	0.4	1.2	$\Phi 12$
$+\alpha$	300	65	0.5	1.4	$\Phi 14$

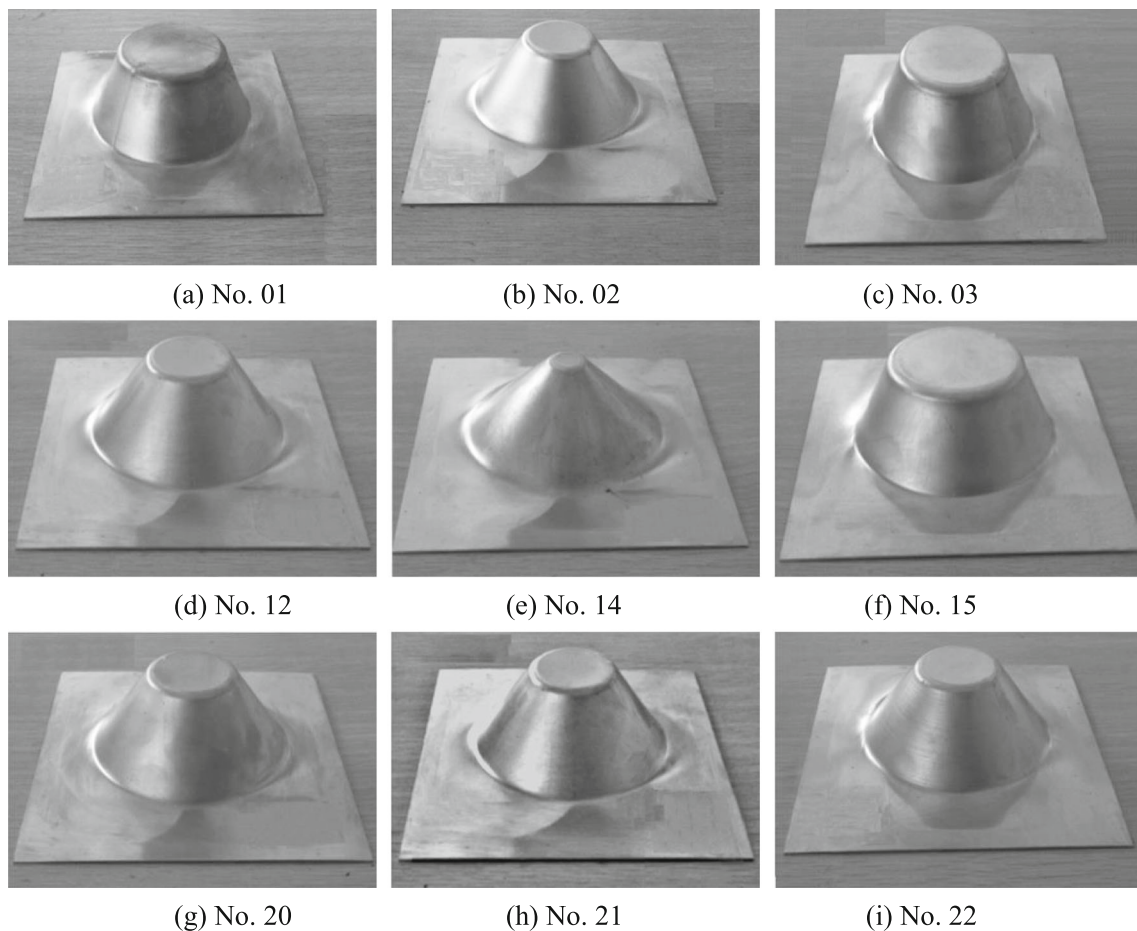


Fig. 5 a–i Some of the final manufactured samples from the WISF assisted with oil bath heating

adopted as the most appropriate model to analyze the springback in the WISF procedure assisted by oil bath heating because it has higher values of the  $F$  value,  $R^2$ ,  $R^2$ -Adj, and  $R^2$ -Pred, and lower values of the  $P$  value and PRESS than those of the other models, as listed in Table 4. The response springback ( $S_s$ ) analyzed by the response surface methodology using a quadratic regression model (black bold font) is expressed by Eq. (3).

$$S_s \text{ (mm)} = +1.74 + 0.13*A + 0.38*B + 0.41*C - 0.25*D + 0.014*E + 0.022*AB - 0.34*AC + 0.180*AD - 0.076*AE - 0.26*BC + 0.27*BD + 7.571e-3*BE + 3.321e-3*CD - 0.16*CE + 0.24*DE - 0.088*A^2 - 0.079*B^2 - 0.096*C^2 - 0.015*D^2 + 1.641e-3*E^2 \quad (3)$$

To investigate the significance of the processing parameters on the aforementioned responses and screen out nonsignificant factors from the considered parameters, ANOVA was used to evaluate the fitness of the adopted model and its terms. Moreover, the adequacies of those models were identified through the coefficient of determination, i.e.,  $R^2$  analysis. The ANOVA and  $R^2$  analysis for Eq. (3) of the springback ( $S_s$ ) quadratic model was performed, and the results are given

in Table 5. A, B, C, and D are the most substantial model terms, while E is the nonsignificant term. From the regression model, it was found that the tool diameter (E) had an adverse effect, while the other variables had a positive effect on the springback ( $S_s$ ). For the quadratic terms, all the rest were the main significant interactive factors affecting the springback ( $S_s$ ), except the interactive terms AB, AE, BE, and CD and the  $D^2$  and  $E^2$  quadratic terms. All significant factors ( $P < 0.5\%$ ) are marked in black bold font in Table 5.

The ANOVA results also disclose that there are more insignificant factors in the model. Reducing the number of insignificant factors from Eq. (3) can simplify the quadratic model. Thus, the model has been modified, and all nonsignificant terms in Table 5 are removed from Eq. (3), except the C term is retained due to the model hierarchical correlation. Finally, the modified quadratic regression model of the springback  $S_s$  in terms of the coded factors is indicated in Eq. (4).

$$S_s \text{ (mm)} = +1.73 + 0.12*A + 0.41*B + 0.42*C - 0.24*D - 3.23*e-3 - 0.32*AC + 0.20*AD - 0.30*BC + 0.22*BD - 0.13*CE + 0.27*DE - 0.086*A^2 - 0.077*B^2 - 0.094*C^2 \quad (4)$$

**Table 3** Design matrix and experimental results

Std	No.	Factor 1 A: $t$ (°C)	Factor 2 B: $\varphi$ (°)	Factor 3 C: $z$ (mm)	Factor 4 D: $h$ (mm)	Factor 5 E: $d$ (mm)	Response 1 $S_y$ (mm)
9	01	250	60	0.2	1.2	$\Phi 8$	2.045
17	02	250	50	0.4	1.2	$\Phi 8$	1.188
21	03	150	60	0.4	0.8	$\Phi 12$	2.046
8	04	250	60	0.4	0.8	$\Phi 8$	2.048
19	05	250	60	0.2	0.8	$\Phi 12$	1.848
4	06	250	50	0.2	1.2	$\Phi 12$	0.858
7	07	150	50	0.4	1.2	$\Phi 12$	1.452
18	08	150	60	0.2	1.2	$\Phi 12$	1.518
1	09	250	50	0.4	0.8	$\Phi 12$	1.386
12	10	150	60	0.4	1.2	$\Phi 8$	1.845
5	11	150	50	0.2	0.8	$\Phi 8$	0.661
15	12	100	55	0.3	1.0	$\Phi 10$	1.122
13	13	300	55	0.3	1.0	$\Phi 10$	1.651
6	14	200	45	0.3	1.0	$\Phi 10$	0.663
24	15	200	65	0.3	1.0	$\Phi 10$	2.178
10	16	200	55	0.1	1.0	$\Phi 10$	0.528
2	17	200	55	0.5	1.0	$\Phi 10$	2.177
26	18	200	55	0.3	0.6	$\Phi 10$	2.173
23	19	200	55	0.3	1.4	$\Phi 10$	1.185
22	20	200	55	0.3	1.0	$\Phi 6$	1.716
14	21	200	55	0.3	1.0	$\Phi 14$	1.772
20	22	200	55	0.3	1.0	$\Phi 10$	1.782
25	23	200	55	0.3	1.0	$\Phi 10$	1.763
16	24	200	55	0.3	1.0	$\Phi 10$	1.726
3	25	200	55	0.3	1.0	$\Phi 10$	1.715
11	26	200	55	0.3	1.0	$\Phi 10$	1.708

To estimate the adequacy of the modified model, ANOVA and  $R^2$  analysis are performed, and the results are listed in Table 6. When the model Prob  $> F$  value is lower than 0.05, it is implied that the model terms are significant. Additionally, when the  $P$  value for the term of the lack of fit is higher than 0.05, it implies that this term is insignificant. Hence, the modified model is significant, and its lack of fit is inconsiderable. The coefficient of determination, i.e., the  $R^2$  value, in this case is 0.9940, which is quite close to 1. This demonstrates that the proposed model has good predictability. The  $R^2$ -Pred of

0.9450 is in reasonable agreement with the  $R^2$ -Adj of 0.9863. This implies that the regression models have high mathematical validity. A signal-to-noise ratio of 39.953, which is greater than 4, represents an adequate signal in the ANOVA. Thus, the modified model can be used to navigate the design space.

Furthermore, the residual is a useful tool for testing the adequacy of the model. It can be defined as the difference between an observed value and its corresponding fitted value for each experimental run. A plot of the normal

**Table 4** Evaluation of the models for the best fit with the experimental results

Source	Std. dev.	$F$ value	$P$ value	$R^2$	$R^2$ -Adj	$R^2$ -Pred	PRESS	Remark
Linear	0.26	13.85	< 0.0001	0.7760	0.7200	0.6001	2.37	
2FI	0.23	1.51	0.2642	0.9106	0.7766	- 3.2972	25.51	
<b>Quad.</b>	<b>0.029</b>	<b>126.94</b>	<b>&lt; 0.0001</b>	<b>0.9993</b>	<b>0.9965</b>	<b>0.9974</b>	<b>0.015</b>	<b>Selected</b>
Cubic	0.032	0.015	0.9064	0.9993	0.9957	—	—	Aliased



**Table 5** The ANOVA and  $R^2$  analysis for Eq. (3) of the sidewall springback  $S_s$  quadratic model

Source	Sum of the squares	df	Mean square	F value	P value (Prob > F)
<b>Model</b>	<b>5.93</b>	<b>20</b>	<b>0.30</b>	<b>357.68</b>	<b>&lt; 0.0001</b>
<b>A-t</b>	<b>0.14</b>	<b>1</b>	<b>0.14</b>	<b>168.70</b>	<b>&lt; 0.0001</b>
<b>B-φ</b>	<b>1.15</b>	<b>1</b>	<b>1.15</b>	<b>1383.67</b>	<b>&lt; 0.0001</b>
<b>C-z</b>	<b>1.36</b>	<b>1</b>	<b>1.36</b>	<b>1639.26</b>	<b>&lt; 0.0001</b>
<b>D-h</b>	<b>0.49</b>	<b>1</b>	<b>0.49</b>	<b>588.47</b>	<b>&lt; 0.0001</b>
E-d	1.568E-003	1	1.568E-003	1.89	0.2276
AB	1.578E-003	1	1.578E-003	1.90	0.2264
<b>AC</b>	<b>0.40</b>	<b>1</b>	<b>0.40</b>	<b>477.22</b>	<b>&lt; 0.0001</b>
<b>AD</b>	<b>0.12</b>	<b>1</b>	<b>0.12</b>	<b>139.63</b>	<b>&lt; 0.0001</b>
AE	0.020	1	0.020	23.57	0.0057
<b>BC</b>	<b>0.23</b>	<b>1</b>	<b>0.23</b>	<b>274.06</b>	<b>&lt; 0.0001</b>
<b>BD</b>	<b>0.24</b>	<b>1</b>	<b>0.24</b>	<b>292.65</b>	<b>&lt; 0.0001</b>
BE	1.943E-004	1	1.943E-004	0.23	0.6488
CD	3.739E-005	1	3.739E-005	0.045	0.8402
<b>CE</b>	<b>0.085</b>	<b>1</b>	<b>0.085</b>	<b>101.95</b>	<b>0.0002</b>
<b>DE</b>	<b>0.19</b>	<b>1</b>	<b>0.19</b>	<b>230.22</b>	<b>&lt; 0.0001</b>
<b>A<sup>2</sup></b>	<b>0.21</b>	<b>1</b>	<b>0.21</b>	<b>253.89</b>	<b>&lt; 0.0001</b>
<b>B<sup>2</sup></b>	<b>0.17</b>	<b>1</b>	<b>0.17</b>	<b>207.07</b>	<b>&lt; 0.0001</b>
<b>C<sup>2</sup></b>	<b>0.25</b>	<b>1</b>	<b>0.25</b>	<b>305.47</b>	<b>&lt; 0.0001</b>
D <sup>2</sup>	5.838E-003	1	5.838E-003	7.04	0.0453
E <sup>2</sup>	7.370E-005	1	7.370E-005	0.089	0.7776
Residual	4.147E-003	5	8.294E-004		
Lack of fit	1.619E-005	1	1.619E-005	0.016	0.9064
Pure error	4.131E-003	4	1.033E-003		
Cor total	5.94	25			
$R^2 = 0.9993$	$R^2_{\text{adjusted}} = 0.9965$	—	$R^2_{\text{predicted}} = 0.9974$	—	—

**Table 6** The ANOVA and  $R^2$  analysis for Eq. (4) of the sidewall springback  $S_s$  quadratic model

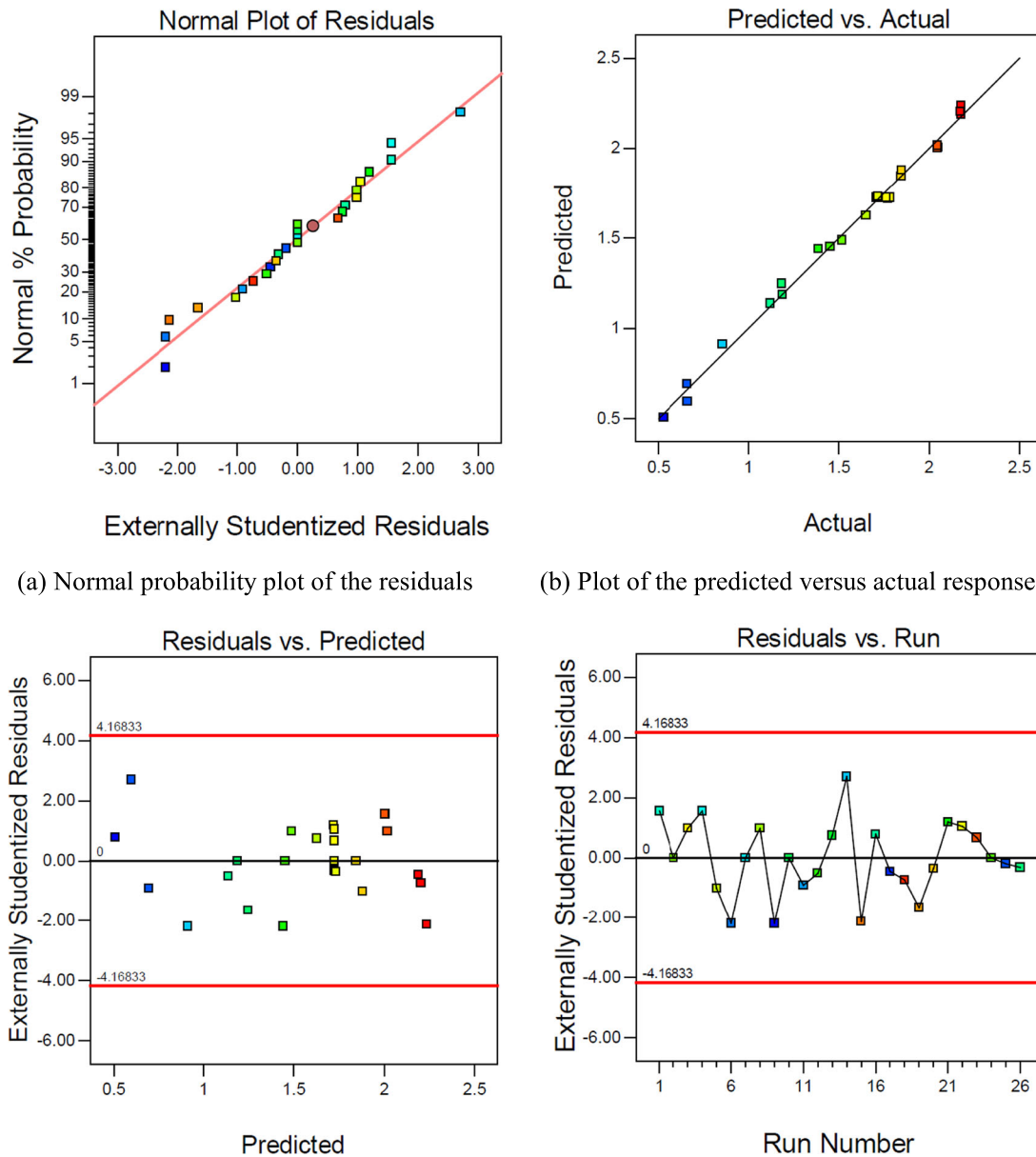
Source	Sum of the squares	df	Mean square	F value	P value (Prob > F)
Model	5.90	14	0.42	129.82	< 0.0001
A-t	0.22	1	0.22	66.84	< 0.0001
B-φ	2.45	1	2.45	755.66	< 0.0001
C-z	1.88	1	1.88	577.84	< 0.0001
D-h	0.61	1	0.61	186.62	< 0.0001
E-d	1.520E-004	1	1.520E-004	0.047	0.8327
AC	0.54	1	0.54	166.19	< 0.0001
AD	0.21	1	0.21	65.36	< 0.0001
BC	0.47	1	0.47	146.16	< 0.0001
BD	0.26	1	0.26	78.97	< 0.0001
CE	0.086	1	0.086	26.55	0.0003
DE	0.36	1	0.36	112.24	< 0.0001
A <sup>2</sup>	0.21	1	0.21	64.46	< 0.0001
B <sup>2</sup>	0.17	1	0.17	52.33	< 0.0001
C <sup>2</sup>	0.25	1	0.25	77.87	< 0.0001
Residual	0.036	11	3.247E-003		
Lack of fit	0.032	7	4.512E-003	4.37	0.0863
Pure error	4.131E-003	4	1.033E-003		
Cor total	5.94	25			
$R^2 = 0.9940$	$R^2_{\text{adjusted}} = 0.9863$	—	$R^2_{\text{predicted}} = 0.9450$	—	—

probability of the residuals for the springback ( $S_s$ ) data and a plot of the actual and predicted responses are presented in Fig. 6 a and b, respectively. The distributions of those data points fall along a straight line, indicating that the data are reliable without a distinct deviation, and suggesting the credibility of the ANOVA and the validity of the simplified regression model. A plot of the residuals versus the predicted responses and a plot of the residuals versus the run number are illustrated in Fig. 6 c and d, respectively. The distributions of those data points show a random pattern of residuals on both sides of the zero line. These results

indicate that the modified model is adequate and qualified to determine the exact relation between the considered parameters and the corresponding response.

### 4.3 Influence of the process parameters on the springback

Here, we independently analyze the effects of the controllable factors and interactive terms on the response and then identify where the effects are derived.



(a) Normal probability plot of the residuals (b) Plot of the predicted versus actual responses (c) Plot of the residuals versus the predicted response (d) Plot of the residuals versus the test run order

Fig. 6 a–d Diagnostic contour plots of the residuals for the sidewall springback ( $S_s$ ) data

### 4.3.1 The effect of a single factor involved multiple interactions

The plots of the main effects of all five influential factors at the midpoint of the levels (i.e., 0 level) in the design space on the springback ( $S_s$ ) are systematically illustrated in Fig. 7.

It can be observed from Fig. 7a that the springback ( $S_s$ ) increases in a quadratic form with an increase in the forming temperature (A). The springback ( $S_s$ ) reaches a critical maximum level at nearly 235 °C and then decreases in a quadratic trend. This is because AZ31B Mg alloy exhibits extremely inferior plastic formability at room temperature. However, with the increase in the forming temperature (A), the non-base slip systems are activated and contribute to the increased ductility of the Mg alloy material, also sharply improving the localized plastic deformation ability of the AZ31B Mg alloy sheet. Once the clamp is released and the temperature decreases, springback ( $S_s$ ) increases gradually. In addition, sharp curvature curves reveal the high sensitivity of the response to the forming temperature (A).

It can be noticed from Fig. 7b that the springback ( $S_s$ ) increases almost linearly with increasing forming angle (B). With the increase in the forming angle (B), the AZ31B Mg alloy material subjected to incremental forming experiences large tension stress due to higher bending strain in the case that the larger forming angle

possesses less material. In other words, due to the increase in the forming angle (B), the material flow during forming is restricted and high tension strain causes a sudden reduction in the thickness. Therefore, after releasing the clamp and decreasing the temperature, a greater retaliatory rebound occurs compared to that with a smaller forming angle. However, an excessively large forming angle (B) leads to early failure of the metal sheet.

It can be seen from Fig. 7c that an increase in the step depth (C) causes an almost linear increase in the springback ( $S_s$ ). At a higher step depth (C), the larger the deformation of the sheet metal per unit area, the larger the equivalent strain within the elastic limit, which results in a larger local springback ( $S_s$ ). Therefore, decreased springback ( $S_s$ ) is obtained when adopting a lower step depth (C). Although a smaller step depth (C) may be able to decrease the springback ( $S_s$ ) during the incremental forming process, the forming time is also greatly increased. Hence, to improve the processing efficiency and meet various processing requirements and conditions, a larger step depth (C) can be used in the case of a larger curvature; otherwise, a smaller step depth can be used for forming parts with a smaller curvature.

It can be discovered from Fig. 7d that the springback ( $S_s$ ) increases almost linearly with decreasing sheet thickness (D). At a larger value of the sheet thickness (D), the deformation of the sheet metal per unit area during the forming process is

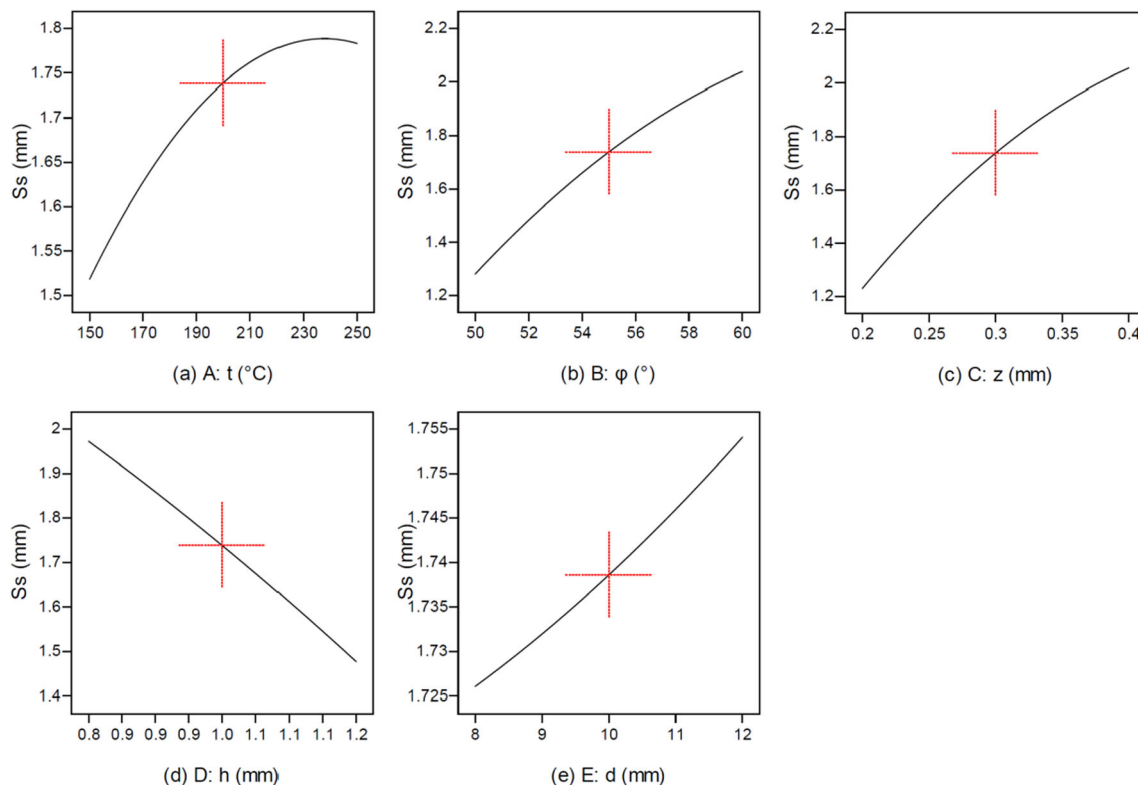


Fig. 7 a–e Main effect plots of five influential factors on the sidewall springback

larger. In particular, the deformation is more than just localized deformation behavior in the contact interface between the tooltip and sheet, and the global deformation behavior of the metal sheet leads to the storage of more deformation energy in the elastic limit range. Therefore, less residual stress is released in a short time after the clamps are released; thus, the springback ( $S_s$ ) decreases. However, if the residual stress is fully released over a long period, the springback still increases with the sheet thickness.

It can be found from Fig. 7e also that an increase in the tool diameter (E) increases the springback ( $S_s$ ) almost linearly. The larger the tool diameter (E), the more residual stress is released when uninstalling the loads; thus, the springback ( $S_s$ ) increases. Moreover, during incremental sheet forming, the interface between the tool and metal sheet is affected by friction because of the sliding and rolling of the tool. When the tool diameter (E) increases, the friction is also higher because the larger areas are subjected to friction. This leads to an increase in the forming temperature (A) and then an increase in the elastic deformation of the material, further increasing the springback ( $S_s$ ).

#### 4.3.2 Response surface results and significant interaction analysis

It can also be observed from Table 6 that there are six interactions that markedly influence the springback ( $S_s$ ) during WISF assisted with oil bath heating. The simultaneous interactive effect of the two independent variables on the springback ( $S_s$ ) is also investigated through the three-dimensional response surface plots while holding the rest of the variables constant at the middle levels of the codes in the design space. The response surface plots of the springback ( $S_s$ ) for the interactions among the independent variables are illustrated in Fig. 8.

**AC interactive term** The response surface plot of the interactive effect for the forming temperature (A) and step depth (C) is demonstrated in Fig. 8a, b. The springback ( $S_s$ ) first increases with the concurrent increase in the forming temperature (A) and step depth (C). However, once the combination of the forming temperature (A) and step depth (C) crosses above the 1.75 contour, the springback ( $S_s$ ) remains nearly constant and reaches its maximum value at a forming temperature (A) of 150 °C and a step depth (C) of 0.4 mm. As indicated before, springback ( $S_s$ ) increases with the forming temperature (A) and then decreases. In addition, the step depth (C) has a more substantial effect on the springback than the forming temperature (A), and the comprehensive action of the two factors leads to such a result. It can be inferred that a low forming temperature (A) and step depth (C) are beneficial for reducing springback ( $S_s$ ).

**AD interactive term** The response surface plot of the interactive effect for the forming temperature (A) and sheet thickness (D) is illustrated in Fig. 8c, d. It is observed that as the forming temperature (A) increases, the springback ( $S_s$ ) also increases slightly. However, the springback ( $S_s$ ) decreases almost linearly with increasing sheet thickness (D). Under the current conditions of the process parameters, the sheet thickness (D) has a more substantial effect on the springback than the forming temperature (A). As explained before, by increasing the sheet thickness, the less residual stress is released in a short time, causing lower stress-induced effects on the sheet metal. Moreover, the oil bath heating approach is also beneficial for improving the homogeneity of the AZ31B Mg alloy sheet, and the probability of homogeneity in the stress distribution increases, which results in lower springback ( $S_s$ ).

**BC interactive term** The response surface plot of the interactive effect for the forming angle (B) and step depth (C) is illustrated in Fig. 8e, f. It is observed that the contours approximate the circumference centered at the origin and diverge to the top right-hand corner, the springback ( $S_s$ ) increases by an increase in both the forming angle (B) and step depth (C), and they have an almost identical effect on the springback ( $S_s$ ). In addition, once they cross above the 1.75 contour, the springback ( $S_s$ ) remains nearly constant and it reaches a maximum value at a forming angle (B) of 60° and a step depth (C) of 0.4 mm. It can be inferred that the small forming angle (B) combined with the low level of the step depth (C) exhibits a lower springback ( $S_s$ ).

**BD interactive term** The response surface plot of the interactive effect for the forming angle (B) and sheet thickness (D) is illustrated in Fig. 8g, h. It is observed that the contours approximate the circumference centered at the origin and diverge to the bottom right-hand corner, the springback ( $S_s$ ) increases by an increase in the forming angle (B) and a decrease in the sheet thickness (D), and both of them have an almost identical effect on the springback ( $S_s$ ). The springback ( $S_s$ ) reaches its maximum value at a forming angle (B) of 60° and sheet thickness (D) of 0.8 mm. It is unfortunate that the forming angle (B) and sheet thickness (D) are recommended to remain constant because both of them are usually predefined in actual production.

**CE interactive term** The response surface plot of the interactive effect for the step depth (C) and tool diameter (E) is illustrated in Fig. 8i, j. It is observed that the contours are approximately parallel lines along the vertical direction. The tool diameter (E) has little effect on the springback ( $S_s$ ). However, the springback ( $S_s$ ) decreases dramatically as the step depth (C) decreases. Although the lower step depth (C) may be able to decrease the springback ( $S_s$ ), the longer forming time is greatly increased. Thus, to improve the

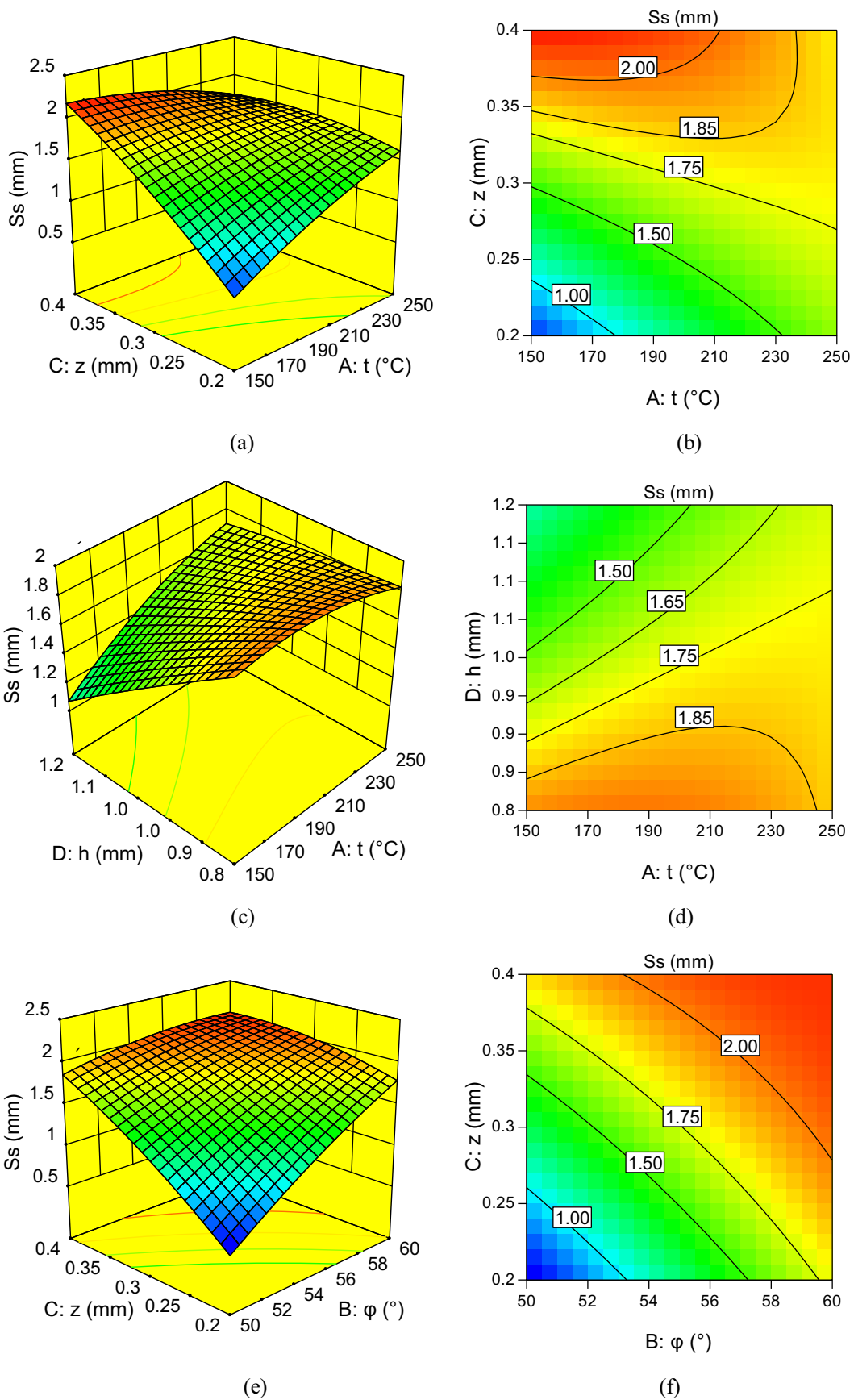


Fig. 8 a–f Three-dimensional response surface plots for the sidewall springback

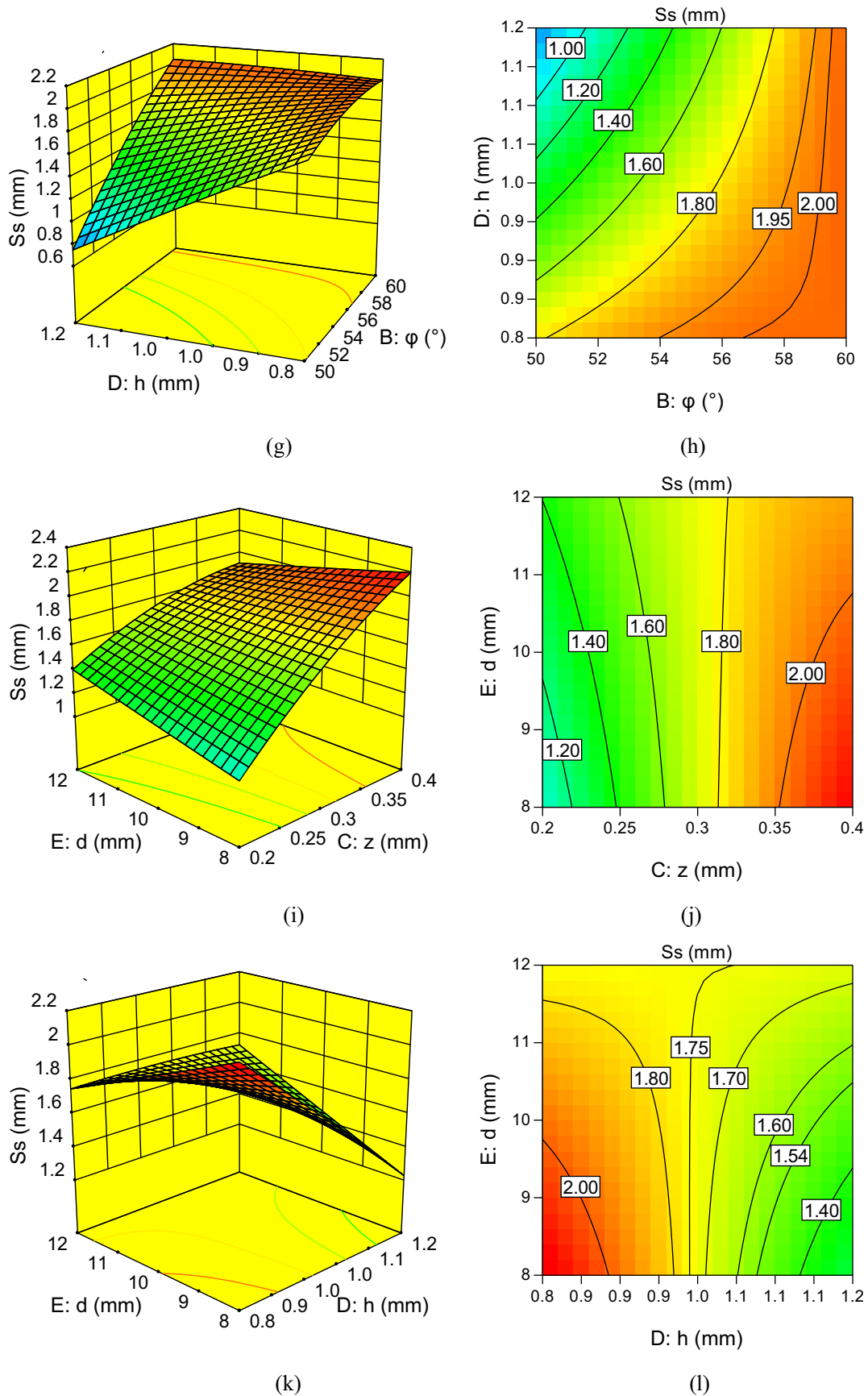


Fig. 8 (continued)

**Table 7** Verification experiments and results for oil bath heating–assisted WISF

No.	A: $t$ (°C)	B: $\varphi$ (°)	C: $z$ (mm)	D: $h$ (mm)	E: $d$ (mm)	Pre. $S_s$ (mm)	Exp. $S_s$ (mm)	$S_s$ error (%)
1	150.0	50.0	0.20	0.8	10.0	0.661	0.687	3.78
2	176.3	50.0	0.20	1.00	10.0	0.314	0.328	4.24
3	182.7	51.5	0.24	1.20	10.0	0.412	0.431	4.41
4	166.3	50.4	0.22	1.18	11.5	0.131	—	—

processing efficiency and meet various processing conditions and requirements, the principle of appropriateness should be adopted in the selection of the step depth (C).

**DE interactive term** The response surface plot of the interactive effect for the sheet thickness (D) and tool diameter (E) is illustrated in Fig. 8k, l. It is observed that their interaction follows the CE interaction. Similarly, the tool diameter (E) has little effect on the springback ( $S_s$ ). As indicated before, the tool diameter (E) is a nonsignificant term in WISF assisted with oil bath heating. The difference is that there seems to be a saddle point where there is an excessive tool diameter (E), i.e., almost greater than 11 mm, and the sheet thickness (D) has a more substantial effect on the springback. This is because if the tool diameter (E) is too large, the contact area, friction resistance, forming force, and surface wear of the forming tool also increase accordingly during the forming process, leading to an increase in the springback ( $S_s$ ).

#### 4.4 Experimental verification and parameter optimization

To validate the aforementioned results, verification experiments were performed, and the optimized process parameters were used for the verification experiments. Springback ( $S_s$ ) using optimization of the RSM in Design Expert 10 trial software was conducted. To acquire the minimal springback ( $S_s$ ), each considered parameter was set to a range from a low to high level, as illustrated in Table 2, and each parameter shared equal importance in this work. In actual production, the sheet thickness is usually predefined, and then the extra constraint for optimization is equal to sheet thicknesses of 0.8, 1.0, and 1.2 mm. For the convenience of the experiment, the tool diameter remained constant at 10 mm because it was a nonsignificant factor for the springback ( $S_s$ ). The experimental runs and verification results are illustrated in Table 7. The experiments were performed within the range of the independent factors, and the relative error was determined by comparing the experimental results with the predicted responses. It was discovered that the average error of the springback ( $S_s$ ) was 4.15% in absolute value. The prediction error was not more than 5% and was within the allowable range. The generated regression model for the springback ( $S_s$ ) could be used to

successfully predict values for the stochastic combination of the forming temperature, step depth, tool diameter, and sheet thickness values within the range of the conducted experiment. The repeatability and reliability of the model for predicting the springback ( $S_s$ ) of incrementally formed AZ31B Mg alloy sheets were obvious. Moreover, without the extra constraint of the sheet thickness and tool diameter, the combination of the process parameters for the optimized value of the minimal springback ( $S_s$ ) was no. 4 in Table 7, yet its verification experimental results are not listed in Table 7 because it is extremely difficult to purchase the commercialized AZ31B Mg alloy sheet at a thickness of 1.18 mm, and the customization cost of the specification is quite expensive and unaffordable for our team. It also shows from another aspect that sheet of the specification is rarely used in actual production. More importantly, the lack of verification experiments may not affect the main conclusions in the present work.

## 5 Conclusions and future work

In the current work, an experimental study on oil bath heating–assisted WISF while forming an Mg alloy (AZ31B) sheet was carried out based on the DOE. The key scientific contribution of the paper was to provide an innovative WISF approach using an oil bath as a heat source. The key technical contribution was to design and fabricate a very simple device with global heating by using an electric heating method at a low cost. Moreover, the response surface modeling analysis based on the CCD method was applied to evaluate, predict, and optimize the springback of the AZ31B Mg alloy in WISF assisted with oil bath heating, and some important findings are summarized as follows:

- (i) The innovative warm incremental sheet forming approach and devices with global heating using an oil bath heating apparatus as a heat source were able to form AZ31B Mg alloy sheets with great reliability and repeatability.
- (ii) The individual effects of five important process parameters on the springback of the AZ31B Mg alloy were investigated, and it was found that the forming temperature, forming angle, step depth, and sheet thickness were

the main significant factors affecting the springback, whereas the tool diameter had a much less influential role on the springback.

- (iii) The interaction effects of the five important process parameters on the springback of the AZ31B Mg alloy were investigated, and it was found that the remaining interactive terms were the main significant interactive factors affecting the springback except for the interactive terms of AB, AE, BE, and CD.
- (iv) It was found that the quadratic regression model gave the best fit with a 95% confidence level for springback, and the repeatability and reliability of the model for predicting the springback of incrementally formed AZ31B Mg alloy sheets were clearly obvious.
- (v) It was found from the optimization that to achieve minimum springback, the 166.3 °C forming temperature, 50.4° forming angle, 0.22-mm step depth, 1.18-mm sheet thickness, and 11.5-mm tool diameter should be selected, and owing to the selection of the parameters, the springback of 0.131 mm should be yielded, although its verification test was not conducted.

The forming quality of the approach is subjected not only to the influence of the previously considered five factors but also to other factors, such as the tool path, feed rate, and spindle speed. In addition, the forming product qualities, such as the sheet thinning and roughness, are also quite important considerations in the commercialization of this innovative approach. However, these phenomena are outside the scope of the paper. Our intent in the present work is simply to shed new light on the feasibility of the warm incremental sheet forming approach with the oil bath heating method. More detailed characteristics will require further investigation in future work.

**Funding information** This work was financially supported by the Department of Science & Technology of Shaanxi Province under Grant No. 2019GY-118; the MOE Key Laboratory of the Thermo-Fluid Science & Engineering under Grant No. KLTFSE2018KF03; the Science & Technology Bureau of the Taizhou City under Grant No. 1701gy27; the National Demonstration Center for Experimental Information & Control Engineering Education under Grant No. 2019ICYB11; and the Xi'an University of Posts & Telecommunications under Grant No. JGZ201816.

## Compliance with ethical standards

**Conflict of interest** The authors declare that they have no conflict of interest.

## References

1. Gang C, Gao J, Yun C, Hong G, Xiang G, Wu S (2017) Effects of strain rate on the low cycle fatigue behavior of AZ31B magnesium alloy processed by SMAT. *J Alloys Compd* 735:536–546. <https://doi.org/10.1016/j.jallcom.2017.11.141>
2. Zhen C, Wang F, Qu W, Zhang Z, Li J, Jie D (2015) Microstructure and mechanical properties of AZ80 magnesium alloy tube fabricated by hot flow forming. *Mater Des* 67:64–71. <https://doi.org/10.1016/j.matdes.2014.11.016>
3. Bao W, Chu X, Lin S, Gao J (2015) Experimental investigation on formability and microstructure of AZ31B alloy in electropulse-assisted incremental forming. *Mater Des* 87:632–639. <https://doi.org/10.1016/j.matdes.2015.08.072>
4. Nguyen NT, Lee MG, Ji HK, Kim HY (2013) A practical constitutive model for AZ31B Mg alloy sheets with unusual stress-strain response. *Finite Elements Anal Des* 76(10):39–49. <https://doi.org/10.1016/j.finel.2013.08.008>
5. Li X, Han K, Xu P, Wang H, Li D, Li Y, Li Q (2020) Experimental and theoretical analysis of the thickness distribution in multistage two point incremental sheet forming. *Int J Adv Manuf Technol* 107(1):191–203. <https://doi.org/10.1007/s00170-020-05037-y>
6. Kulkarni SS, Mocko GM (2020) Experimental investigation and finite element modeling of localized heating in convective heat-assisted single-point incremental forming. *Int J Adv Manuf Technol* 107(1):945–957. <https://doi.org/10.1007/s00170-020-05082-7>
7. He A, Kearney MP, Weegink KJ, Wang C, Liu S, Meehan PA (2020) A model predictive path control algorithm of single-point incremental forming for non-convex shapes. *Int J Adv Manuf Technol* 107(1):123–143. <https://doi.org/10.1007/s00170-020-04989-5>
8. Duc-Toan N, Yang SH, Dong-Won J, Tien-Long B, Young-Suk K (2012) A study on material modeling to predict spring-back in V-bending of AZ31 magnesium alloy sheet at various temperatures. *Int J Adv Manuf Technol* 62(5-8):551–562. <https://doi.org/10.1007/s00170-011-3828-y>
9. Mcanulty T, Jeswiet J, Doolan M (2017) Formability in single point incremental forming: a comparative analysis of the state of the art. *CIRP J Manuf Sci Technol* 16:43–54. <https://doi.org/10.1016/j.cirpj.2016.07.003>
10. Li Y, Chen X, Liu Z, Jie S, Li F, Li J, Zhao G (2017) A review on the recent development of incremental sheet-forming process. *Int J Adv Manuf Technol* 2:1–24. <https://doi.org/10.1007/s00170-017-0251-z>
11. Yang DY, Bambach M, Cao J, Dufflou JR, Groche P, Kuboki T, Sterzing A, Tekkaya AE, Lee CW (2018) Flexibility in metal forming. *CIRP Ann* 67(2):743–765. <https://doi.org/10.1016/j.cirp.2018.05.004>
12. Jeswiet M, Hirt B, Dufflou (2005) Asymmetric single point incremental forming of sheet metal. *CIRP Ann Manuf Technol* 54(2): 88–114. [https://doi.org/10.1016/S0007-8506\(07\)60021-3](https://doi.org/10.1016/S0007-8506(07)60021-3)
13. Ambrogio F, Manco GL (2008) Warm incremental forming of magnesium alloy AZ31. *CIRP Ann Manuf Technol* 57(1):257–260. <https://doi.org/10.1016/j.cirp.2008.03.066>
14. Wang W, Lei H, Tao K, Chen S, Wei X (2015) Formability and numerical simulation of AZ31B magnesium alloy sheet in warm stamping process. *Mater Des* 87:835–844. <https://doi.org/10.1016/j.matdes.2015.08.098>
15. Wong TW, Hadadzadeh A, Wells MA (2017) High temperature deformation behavior of extruded AZ31B magnesium alloy. *J Mater Process Technol* 251:360–368. <https://doi.org/10.1016/j.jmatprotec.2017.09.006>
16. Al-Obaidi A, Kräusel V, Landgrebe D (2016) Hot single-point incremental forming assisted by induction heating. *Int J Adv Manuf Technol* 82(5-8):1163–1171. <https://doi.org/10.1007/s00170-015-7439-x>
17. Balasubramanian S, Anand L (2002) Plasticity of initially textured hexagonal polycrystals at high homologous temperatures: application to titanium. *Acta Mater* 50(1):133–148. [https://doi.org/10.1016/S1359-6454\(01\)00326-3](https://doi.org/10.1016/S1359-6454(01)00326-3)



18. Balamurugan KG, Mahadevan K (2015) Investigation on the effects of process parameters on the mechanical and corrosion behaviour of friction stir-clad AZ31B magnesium alloy. *Arab J Forence Eng* 40(6):1647–1655. <https://doi.org/10.1007/s13369-015-1623-z>
19. Duflou JR, Habraken A-M, Cao J, Malhotra R, Bambach M, Adams D, Vanhove H, Mohammadi A, Jeswiet J (2018) Single point incremental forming: state-of-the-art and prospects. *Int J Mater Form* 11(6):743–773. <https://doi.org/10.1007/s12289-017-1387-y>
20. Xu DK, Lu B, Cao TT, Zhang H, Chen J, Long H, Cao J (2016) Enhancement of process capabilities in electrically-assisted double sided incremental forming. *Mater Des* 92:268–280. <https://doi.org/10.1016/j.matdes.2015.12.009>
21. Liu Z (2018) Heat-assisted incremental sheet forming: a state-of-the-art review. *Int J Adv Manuf Technol* 98(5):2987–3003. <https://doi.org/10.1007/s00170-018-2470-3>
22. Reese ZC, Ruszkiewicz B, Nikhare CP, Roth JT (2015) Effect of toolpath on the springback of 2024-T3 aluminum during single point incremental forming. In: *Asme International Conference on Manufacturing Science & Engineering*. <https://doi.org/10.1115/MSEC2015-9438>
23. Zhu H, Chang X, Jung DW (2018) The generation of the forming path with the springback compensation in the CNC incremental forming. *Int J Mater Form* 11(4):455–470. <https://doi.org/10.1007/s12289-017-1355-6>
24. Wang H, Zhang R, Zhang H, Qi H, Chen J (2018) Novel strategies to reduce the springback for double-sided incremental forming. *Int J Adv Manuf Technol* 9:1–7. <https://doi.org/10.1007/s00170-018-1659-9>
25. Khan MS, Coenen F, Dixon C, El-Salhi S, Penalva M, Rivero A (2015) An intelligent process model: predicting springback in single point incremental forming. *Int J Adv Manuf Technol* 76(9-12):2071–2082. <https://doi.org/10.1007/s00170-014-6431-1>
26. Ajay K, Vishal G (2019) Experimental investigation and optimization of surface roughness in negative incremental forming. *Measurement* 131:419–430. <https://doi.org/10.1016/j.measurement.2018.08.078>
27. Mostafanezhad H, Menghari HG, Esmaeili S, Shirkharkolaee EM (2018) Optimization of two-point incremental forming process of AA1050 through response surface methodology. *Measurement* 127:21–28. <https://doi.org/10.1016/j.measurement.2018.04.042>
28. Li Y, Lu H, Daniel WJT, Meehan PA (2015) Investigation and optimization of deformation energy and geometric accuracy in the incremental sheet forming process using response surface methodology. *Int J Adv Manuf Technol* 79(9-12):2041–2055. <https://doi.org/10.1007/s00170-015-6986-5>
29. Balajii M, Niju S (2019) A novel biobased heterogeneous catalyst derived from *Musa acuminata* peduncle for biodiesel production-process optimization using central composite design. *Energy Convers Manag* 189:118–131. <https://doi.org/10.1016/j.enconman.2019.03.085>
30. Ahmad T, Danish M, Kale P, Geremew B, Adeloju SB, Nizami M, Ayoub M (2019) Optimization of process variables for biodiesel production by transesterification of flaxseed oil and produced biodiesel characterizations. *Renew Energy* 139:1272–1280. <https://doi.org/10.1016/j.renene.2019.03.036>

**Publisher's note** Springer Nature remains neutral with regard to jurisdictional claims in published maps and institutional affiliations.